Rheological Behavior of Inconel 718 Powder for Electron-Beam Melting

metals

MDPI

Article

Rheological Behavior of Inconel 718 Powder for Electron-Beam Melting

Laura Cordova *, Ahmad Raza and Eduard Hryha

Department of Industrial and Materials Science, Chalmers University of Technology, 41296 Gothenburg, Sweden; ahmadra@chalmers.se (A.R.); hryha@chalmers.se (E.H.)

* Correspondence: laura.cordova@chalmers.se

Abstract: Understanding the impact of powder reuse in powder-bed-fusion electron beams (PBF-EB) is key to maintain the processability and yield. Powder oxidation, due to exposure to high temperatures for a prolonged period of time, can lead to a decrease in electrical conductivity of the powder and, hence, electrostatic forces that originate during interaction with the electron beam. The effect of oxidation on physical properties as powder rheological properties, apparent/tap density and charging are studied in this work. The analysis using Scanning Electron Microscopy (SEM) shows thermodynamically stable Al-rich oxide particulates (sized 100–200 nm) covering the surface of the reused powder particles, with an increase of 20% in bulk oxygen in comparison to the virgin powder and, measured by X-ray Photoelectron Spectroscopy (XPS), average oxide thickness of circa 13 nm in the reused powder. On the one hand, reusing the powder positively impacted the flowability studied using the Revolution Powder Analyzer (RPA), in which the avalanche angle was decreased from 37 deg to 30 deg, for virgin and reused powder, respectively. The volume fraction of loose powder was similar for both virgin and reused powder, 57% and 56%, respectively, while the packed volume fraction was measured lower in the reused (57%) than the virgin powder (60%). On the other hand, the charging behavior, studied using the ION Charge Module of the powder, worsened; this almost doubled in the reuse powder (−9.18 V/g) compared to the virgin powder (−5.84 V/g). The observation of ejected particles from the build volume is attributed to the charging behavior and lower packing volume fraction in the reused powder.

Keywords: powder reuse; electron beam melting; PBF-EB; Inconel 718; surface chemistry; powder rheology; particle charging

Citation: Cordova, L.; Raza, A.; Hryha, E. Rheological Behavior of Inconel 718 Powder for Electron-Beam Melting. *Metals* **2022**, *12*, 1231. https://doi.org/10.3390/met12071231

Academic Editor: Pavel Krakhmalev

Received: 25 May 2022
Accepted: 19 July 2022
Published: 21 July 2022

1. Introduction

In recent times, metal additive manufacturing processes have become popular beyond rapid prototyping. The powder-bed fusion group of processes, including laser beam (PBF-LB) and electron beam (PBF-EB), are widely used for the fabrication of industrial goods requiring high design complexity and low-volume batches. Most of the applications for the PBF-EB process require high purity, repeatability, and defect-free parts. For example, the aerospace industry, for structural and rotating parts, demands low content of interstitials, defects and contamination that could compromise the performance in operating conditions. Inconel 718, being one of the early adopted materials in PBF processes, is one of the most demanded, given its high strength, corrosion resistance, welding processability and wide operating temperatures (up to 650 °C) [1,2].

The PBF-EB process consolidates powder particles into 3D objects obtained from a computer-aided-design (CAD) file [3]. In PBF-EB, the electron beam serves as an energy source that preheats and melts the powder particles under a high vacuum to protect powders from oxidation [4]. The PBF-EB process starts with raking the powder particles onto a substrate layer by layer, forming the powder bed. Homogeneous spreadability of the powder is necessary for good powder packing. This is followed by a preheating step,

in which the deposited layer is scanned with a low-power density electron beam. Due to the high pre-heating temperature (close to 1000 °C for Inconel 718), the parts are to be extracted from a partially sintered powder 'cake'. In fact, powder sintering relies on high thermal and electrical conductivity between metal particles. The electrons, in the case of poor electrical conductivity of the powder cake, can accumulate on the powder surface and grow electrostatic repulsion forces, which can lead to the smoking effect, a term used when particles are ejected from the build envelope by powder–beam interaction [5]. This effect does not occur often when melting if not observed previously during the pre-heating stage. The smoking effect must be avoided since it is usually a source of build failure.

After melting with a focused electron beam and cooling down the build chamber, the built part can be extracted. Since most of the powder used that surrounds the part has not been melted, it can be recovered for subsequent build cycles. This recovery process makes use of grit blasting to separate agglomerates of powder particles and to mix the heat-affected powder with powder from the hoppers that were not exposed to the process. The recovered powder can be loaded into the hoppers to restart the PBF-EB process. This results in a mix of powders with different thermal history. Given the high temperatures at which the PBF-EB process takes place, the surface chemistry of the powder particles can vary with an increasing number of reuse cycles and, consequently, the thickness of the oxide layer, as described by Hryha et al. [6] in a different study. Surface chemistry is one of the key properties linked to charging, since the oxide layer that surrounds the powder particle acts as a dielectric layer and, hence, determines the electrical properties of the powder bed; this effect was simulated by Chiba et al. [7].

Ensuring part repeatability, even at high reuse cycles, is key for process cost effectiveness and sustainability. Reusability studies of Inconel 718 in PBF-EB are limited in comparison with other materials (e.g., Ti-6Al-4V) and AM techniques (e.g., PBF-LB). Powder reuse in PBF-LB has reported pick up of oxygen and improved values in flowability of Inconel 718 powder, with no detrimental effect in the mechanical properties [8,9]. However, the oxidation mechanisms and process conditions in PBF-EB are different than other metal AM processes. In PBF-EB, the high vacuum protects the powder from oxidation at high temperatures, although upon reuse of the powder, oxidation will take place, generating Al-rich oxides, as studied by Gruber et al. [10]. As observed, as well, by Raza et al. [11], in the PBF-EB working conditions, the sublimation pressure of the oxides for the elements Ni, Cr and Al are lower than of pure metals, in which Al has the highest equilibrium sublimation pressure, followed by Cr. In a following study by Gruber et al. [12], surface oxidation was correlated to defect formation, in which the Al-rich oxides deposited on the reused powder particles will tend to cluster in the liquid metal, solidifying as inclusions. The effect of the impact using Charpy V-notch (CVN) test samples of virgin and reused Inconel 718 powder processed by PBF-EB was studied by Gruber et al. [13]. The conclusion is a large heterogeneity of fracture features in both variations of powder (virgin and reused), with dominated by Al-rich oxides films and non-metallic inclusions.

Most reusability studies covering different materials are still based on traditional flowability testing methods used in powder metallurgy, such as Hall and Carney flowmeters, which are only suitable for a free-flowing powder subjected to gravitational forces. However, these methods have been questioned repeatedly in the PBF process, given the thin-layer application requirements [14,15]. Alternatively, more advanced rheological equipment has been used to characterize metal powder, in particular, Freeman FT4, and rotation drum analyzers offer quantifiable measurement capabilities [16–18]. Spreading devices to mimic the powder-bed application have been also used to characterize powder in various conditions [19,20]. While the effect of reuse on the surface chemistry of Inconel 718 powder has been investigated before, the impact of this on the rheological behavior and charging of the powder bed have not been addressed to the best of our knowledge. In this work, we use X-ray photoelectron spectroscopy (XPS) to study the surface oxide chemistry of virgin and reused powder particles, which can have a strong influence not only on the charging behavior of the powder in the process but also its spreadability. Rheo-

logical properties of the powders under different regimes and speed conditions using the rotation drum principle are studied and linked to the spreading speed of the raking device in PBF-EB.

2. Materials and Methods

The Inconel 718 atomized powder was supplied by Arcam AB, Mölndal, Sweden, with composition as listed in Table 1 and particles between 45 and 115 µm (Figure 1a,b). Two variations of the same powder were studied, in virgin and reused state. The virgin powder refers to the material that is freshly atomized and has not been processed yet, while the reused powder has been part of the process for multiple build cycles and has been discarded due to smoking during PBF-EB processing and is, hence, unsuitable for reuse.

Table 1. Composition of Inconel 718 powder.

Elements	Ni	Co	Cr	Mo	Ti	Mn	Nb	Ta	Al	Fe	Si	C
wt.%	54.1	0.04	19.0	2.99	1.02	0.12	4.97	<0.01	0.52	17.12	0.06	0.03
at%	53.38	0.04	21.16	1.80	1.23	0.13	3.10	<0.01	1.12	17.75	0.12	0.14

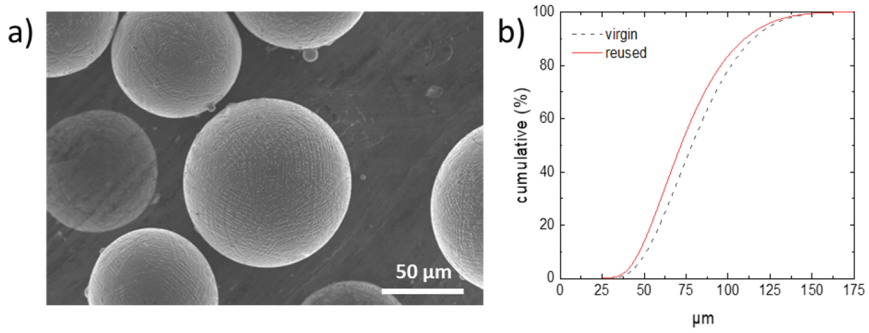

Figure 1. Inconel 718 powder (**a**) morphology of the virgin powder and (**b**) particle size distribution of virgin and reused powders.

The particle surface morphology of the samples was studied by high-resolution scanning electron microscopy (HR-SEM) using a Carl ZEISS-LEO Gemini 1550 SEM microscope (ZEISS Microscopy, Jena, Germany), equipped with a field emission gun. The bulk oxygen and nitrogen content of the virgin and reused powder samples were measured by a hot fusion analysis using an ON836 instrument (LECO, St. Joseph, MI, USA). The particle size distribution was measured by laser diffraction using an HELOS (Sympatec, Clausthal-Zellerfeld, Germany) with an RODOS dry-disperser analyzer. To measure the moisture content on the particle surface, thermogravimetric analysis was performed using a thermal analyzer STA449 (NETZSCH Thermal Analysis GmbH, Bayern, Germany). A calibration testing curve using only alumina filler was subtracted from the measurement to eliminate the effect of the gas flow and improve measurement accuracy. The samples were heated from room temperature to 300 °C with a heating rate of 10 K/min followed by an isothermal for 60 min under scientific purity (99.9999%) argon gas atmosphere.

The rheological behavior of virgin and reused Inconel 718 powder was studied by the rotation drum principle using a Revolution Powder Analyzer (RPA) by Mercury Scientific Inc (Newtown, CT, USA). The test is carried on a rotating and transparent drum filled with powder. A camera in front of a light source records pictures of the powder surface area on movement. An image analysis software converts the image in different parameters associated with powder flowability. Given the rotation of the drum, the powder is carried up the side of the drum causing it to collapse or avalanche by its own weight. The test is designed to characterize the avalanche angle which flows in similar manner as powder spreading during layer-based application in PBF processes, and, hence, allows one to evaluate particle-to-particle and particle-to-base plate interactions. Equal sample size of

110 g of virgin and reused material was freely loaded in the drum. The rheological and charging tests were performed at atmospheric conditions of 26 °C and 43 RH%. Sample drying was performed ex situ at 100 °C for 2 h. For the flowability measurements a constant speed of 0.6 RPM was selected in which 150 powder avalanches were analyzed. Additionally, a separate experiment varying speed from 1 to 70 RPM was set in which 75 avalanches were analyzed for each angular speed. The selection of the speed range was based on the recoater linear speed of about 250 mm/s which is equivalent to an angular speed of 48 RPM as per Equation (1).

$$w = \frac{V_L}{2\pi R} \times 60 \text{ [RPM]} \quad (1)$$

where w is the angular speed, V_L is the linear speed of the recoater and R the radius of the revolution powder analyzer.

The tap density was obtained by the packing test which consists of vibrating the rotation drum repeatedly for ten cycles, ρ_{Tap} is the average of ten measurements. This is divided by $\rho_{Theoretical}$, in this case 8.2 g/cm^3, to obtain the relative density as in Equation (2).

$$R = \frac{\rho_{Tap}}{\rho_{Theoretical}} [\%] \quad (2)$$

Using the ION Charge Module integrated in the RPA, the powder-charging properties are studied. Measuring the charging properties of PBF-EB powder is important, especially upon reuse, given potential changes in the oxide layer. The measurements were taken both during rotation at a constant speed of 10 RPM and during decay in static mode. Before the measurements, the drum is thoroughly cleaned with a solution of 90% Isopropanol and 10% water and gently dried with a paper towel. This is followed by deionizing of all the parts of the drum including both sides of the polycarbonate transparent lids and metal cylinder for 30 s. This procedure is carried out to improve accuracy since electrostatic charge measurements are very sensitive to handling.

For surface analysis, X-ray photoelectron spectroscopy (XPS) was conducted using PHI 5500 (Physical Electronics, Chanhassen, MN, USA) equipped with a monochromator Al Kα source. The samples for the measurement were prepared on a 3M carbon tape substrate. To obtain statistically authentic data, the analysis area for measurement was 300 µm × 300 µm. The pass energy used for the survey and the narrow elemental scans was 226 eV and 69 eV, respectively. For the depth profile analysis, Ar + ions were used to etch the sample surface. The etch depth was calibrated on Ta_2O_5 foil, and all the information about etching depth is as per that standard. The obtained data were analyzed using the MultiPak 9.7.0.1 software provided by PHI.

3. Results

3.1. Morphological Characterization

The SEM micrographs in Figure 2 show large differences in the surface morphology of the virgin and reused powder particles. The dendrites formed during atomization observed in the virgin particles cannot be perceived anymore in the reused powder particles; instead, bright particulates cover most of the surface. These were identified by Gruber et al. [10] as Al-rich oxide inclusions, with sizes between 50 nm and 200 nm, and they constitute the dominant part of the oxide layer of the reused powder particles. The size of the particulates, as shown in Figure 2b3, is also estimated between 100 nm and 200 nm. More detail into these particulates is found in Figure 2b3. Most reused powder particles exhibit bumps and deformations (Figure 2b1), associated to the blasting step used to separate the powder cake formed when sintering the powder bed in PBF-EB, where temperatures reach up to 1000 °C for Inconel 718.

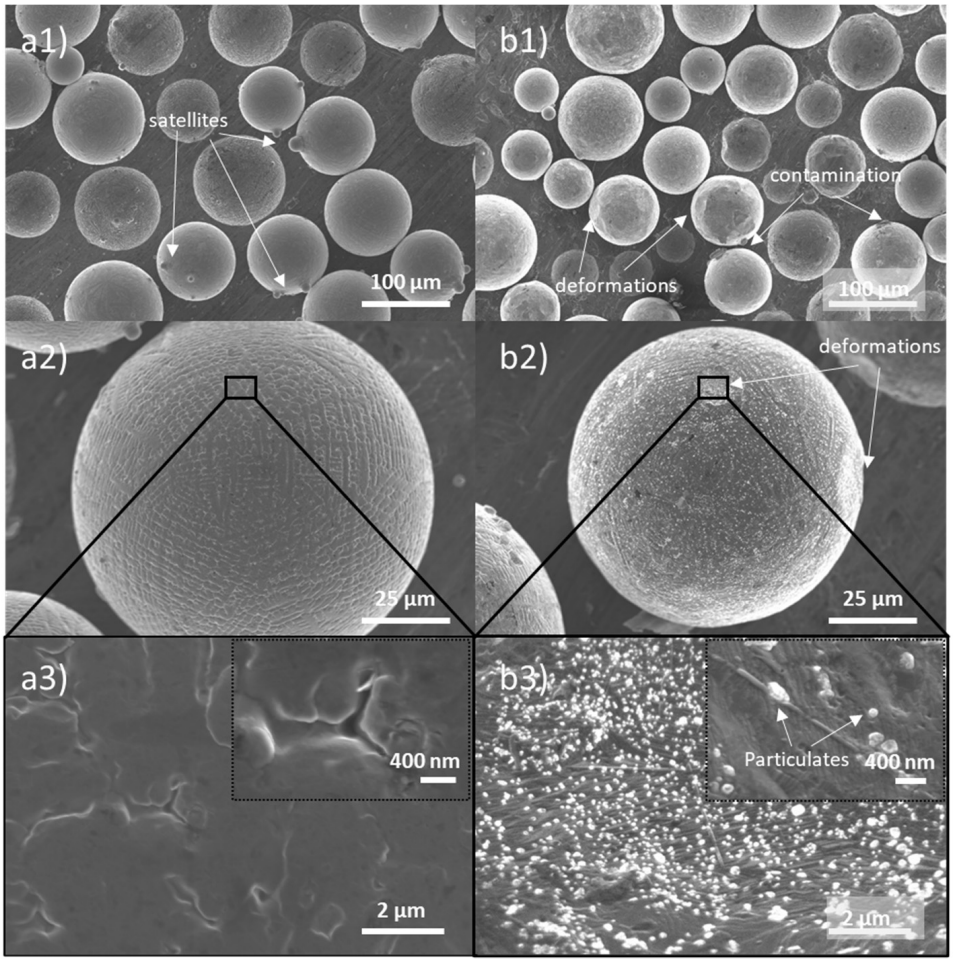

Figure 2. SEM micrographs of surface of virgin powder at 500, 2000 and magnifications, respectively, (**a1**–**a3**) and reused powder (**b1**–**b3**). Inserts in (**a3**,**b3**) at 100 K show presence of particulate oxide sizing up to 100 nm in case of reused powder and clean surface in case of virgin powder.

The pre-sintering step carried out in PBF-EB before melting is aiming to sinter powder particles into a powder cake to assure necessary thermal and electrical conductivity and avoid smoking. When blasting the feedstock for reuse, some of these agglomerates, with sizes smaller than the sieving mesh, can remain in the reused powder, as observed in Figure 3. Analysis of these agglomerates show that oxidation is very pronounced in the interparticle necks, as shown in Figure 3c.

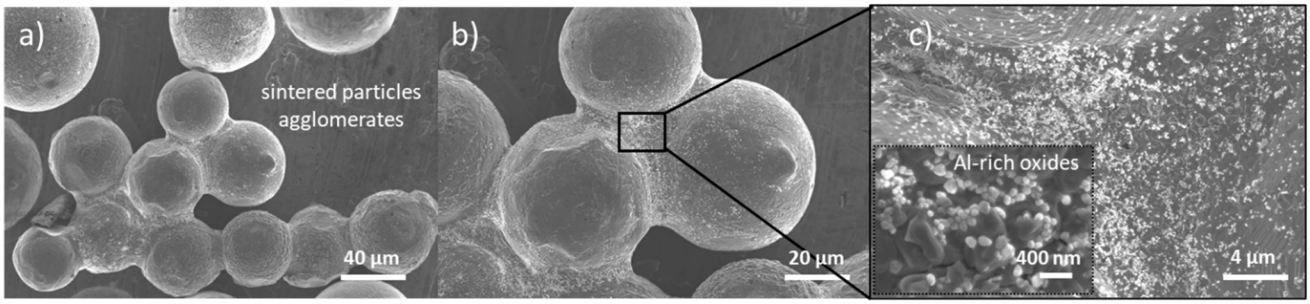

Figure 3. Oxidation of powder in the sintered cake: (**a**) agglomerate of particles found in reused powder, (**b**) interparticle necks formed during sintering and (**c**) Al-rich oxides observed at the interparticle necks.

3.2. Bulk Chemical Analysis and Particle Size Distribution

Bulk composition of nitrogen, oxygen and humidity contents (estimated by thermogravimetry analysis), in addition to particle size, D10, D50 and D90 metric values of virgin and reused powder, are listed in Table 2. Given the vacuum conditions of the PBF-EB process, most oxygen pick-up can be avoided, although not completely, since the powder is handled outside the machine in between reuse cycles. The oxygen content shows some oxygen pick-up, indicating powder oxidation, in line with the SEM observation of the powder surface, see Figures 2 and 3. The moisture in the virgin powder appears to have decreased its initial weight upon drying more than the reused powder; the total mass loss is 0.5 mg and 0.4 mg, respectively, as indicated in Table 2. No large differences in mass loss are observed since both powders were kept in similar storage conditions before characterization.

Table 2. Nitrogen and oxygen content determined by inert gas fusion and moisture measured by thermogravimetry analysis.

Material	O (%)	H_2O (%)	D10 (µm)	D50 (µm)	D90 (µm)
virgin	0.0153	0.0255	51.73	78.32	113.90
reused	0.0184	0.0229	47.30	71.45	108.98

The PSD curve, as plotted in Figure 1, and particle size metrics D10, D50 and D90 (Table 2) show a minor decrease in particle size in the reused powder when compared to the virgin powder. PSD influences the general powder flowability and, more specifically, the spreadability in thin-layer application, as required by PBF processes. In general, wider PSD has a positive effect in the powder packing since smaller particles tend to fill larger interparticle spaces helping to achieve higher densification. Additionally, fine particles sinter faster, enabling powder cake formation and better electrical conductivity of the powder layer during melting with the electron beam.

3.3. Surface Chemical Analysis

XPS survey spectra are useful to observe variations in the surface chemistry of different samples. Survey spectra of virgin and reused Inconel 718 powders are presented in Figure 4. Although the relative peak intensities are varying, peaks of elements, such as oxygen (O1s), carbon (C1s), Ni (2p), Cr (2p), niobium (Nb3d) and titanium (Ti2p), are present in both virgin and reused powder. A slight decrease in the Ni2p peak intensity can be observed in the spectra obtained from the reused powder compared to the virgin powder. Contrarily, an increase in the intensity of the Ti2p peak can be observed in the reused powder. Moreover, a noticeable difference between the virgin and the reused spectra is in the appearance of the Al peak in the case of the reused powder, which was not present in the virgin powder. It indicates that the surface of the reused powder is enriched in Al, which is an indication of possible formation of Al-based oxides as observed in the SEM micrographs (Figure 2). A decrease in relative intensity of Ni2p and an increase in the intensities of Al2s and Ti2p can be an indication of a shift of oxygen from less stable oxides (i.e., Ni, Fe) to more stable oxides (i.e., Ti, Al) during processing in the PBF-EB process.

To further investigate the nature and variation in surface chemistry upon reuse of metal powder, depth profile analysis was conducted. Figure 5 shows a comparison of the depth profile of the dominant oxide-forming elements in Inconel 718, including Al, Cr and Ti. A distinguishable difference between the Al spectra of virgin and reused powder can be observed, in which the spectra in case of virgin powder only shows a peak with minute intensity at the as-received surface at 119.5 eV, representing Al-based hydroxides present on the as-received surface. On a slightly etched surface of virgin powder, the Al peak disappeared. Contrarily, the reused powder shows a pronounced Al peak at 119.8 eV, representing the formation of Al-based oxides. This peak is present even at the etched depth of 30 nm, indicating the coarser nature of Al-based oxides. These findings are in

agreement to the observed surface morphology of the powder, in which particulates of up to 200 nm are present on the surface of the reused powder.

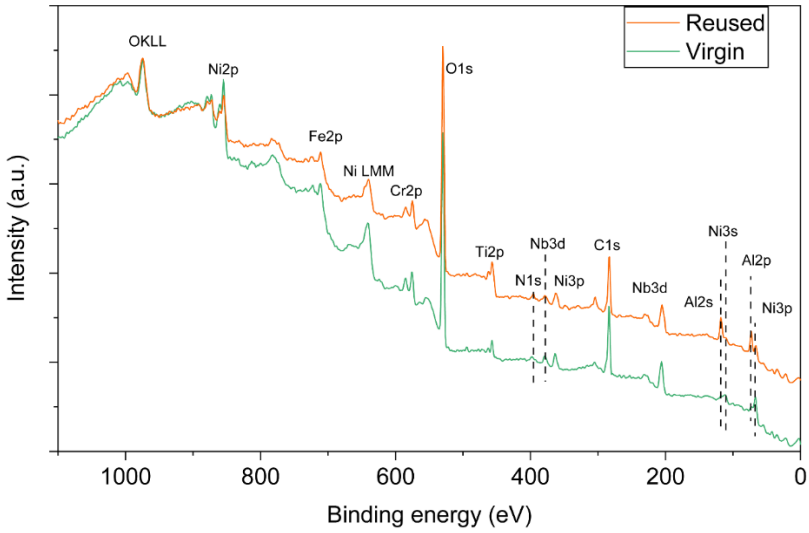

Figure 4. XPS survey spectra of virgin and PBF-EB reused Alloy 718 powder.

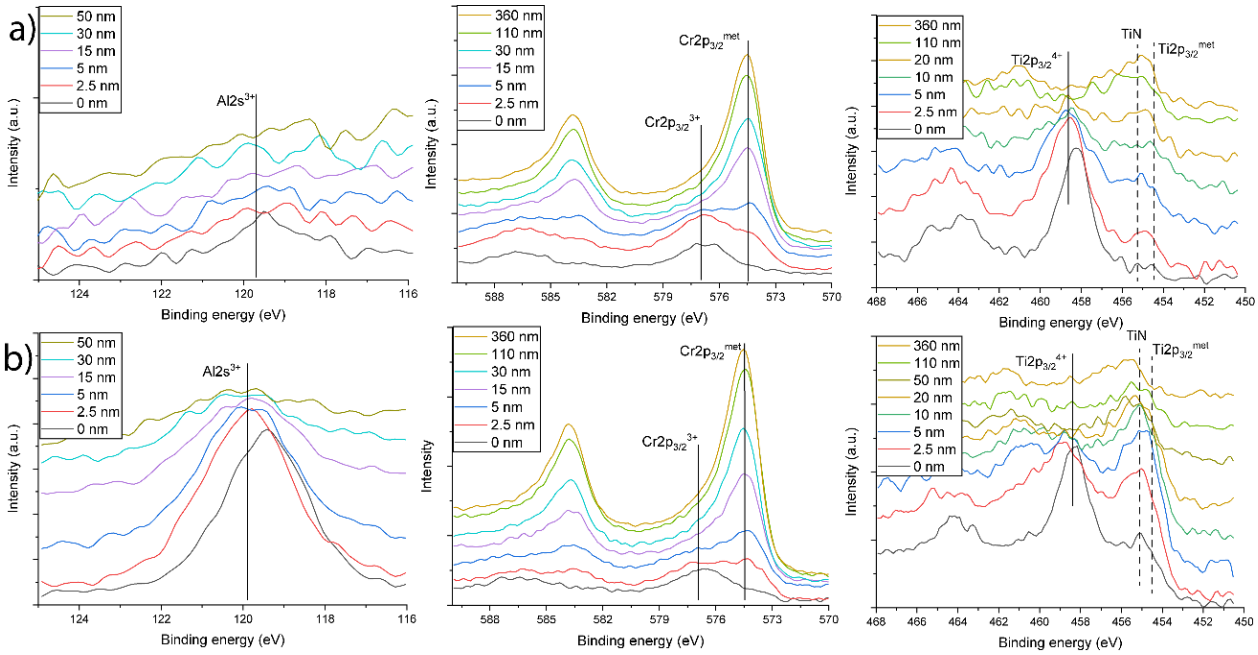

Figure 5. Comparison of depth profile of Al2s, Cr2p and Ti2p spectra for (**a**) virgin and (**b**) reused powder.

The trend is a little different in the case of Cr2p spectra, where the $Cr2p_{3/2}{}^{met}$ peak dominated the $Cr2p_{3/2}{}^{3+}$ at the etched depth of 5 nm in virgin powder. In the case of reused powder, the $Cr2p_{3/2}{}^{met}$ peak already dominated the $Cr2p_{3/2}{}^{3+}$ peak at 2.5 nm etched depth. This shift in $Cr2p_{3/2}$ from oxide to metal state with powder reuse is highlighting redistribution of oxygen at high-temperature conditions during PBF-EB processing, from less stable to more stable oxide-forming element. Therefore, it can be hypothesized that the oxygen used by Al to form Al-based oxides was obtained from preexisting oxides (e.g., Ni, Fe, Cr) on the surface of virgin powder. Gruber et al. [10] also observed such redistribution while analyzing the variations in surface chemistry of Inconel 718 powder by reuse in the PBF-EB process. Comparison of narrow scans from Ti2p show an increase in TiN in reused

powder compared to virgin powder, which explains the appearance of the N peak in survey spectra of reused powder.

Normalized oxygen intensity, calculated from O1s spectra, can be useful to see the change in the profile of oxygen distribution, see Figure 6a. The reused powder sample shows higher normalized oxygen intensity compared to virgin powder until ~100 nm etched depth. This increase in oxygen content with etched depth is originated from the presence of oxide particulates on the surface of the reused powder. Figure 6b shows the average thickness of oxide particulate phases determined by using the intensity of O1s spectra [21]. The point where the intensity of O1s decreased to 50% of its peak intensity was considered as an interface. The average thickness of oxide particulates estimated using this methodology in the case of virgin powder was ~7.66 nm and for reused powder was ~12.86 nm.

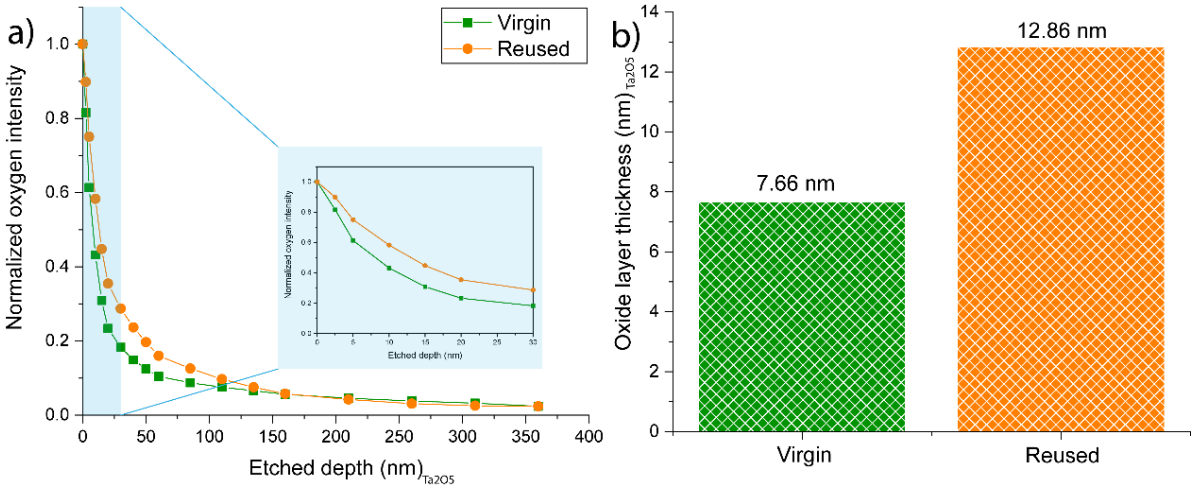

Figure 6. Comparison of (**a**) variation in normalized oxygen intensity with etched depth and (**b**) average oxide particulate/layer thickness for virgin and reused powder calculated by using O1s spectra. Depth is measured relative to the etch rate of Ta_2O_5, which was used to calibrate the etch rate.

3.4. Rheological Behavior

The rheological behavior of metal powders plays a key role in successful application of the thin layer prior to sintering and melting in PBF-EB [19]. Thus, the packing density of the powder layer will enable a full contact between particles for higher electrical conductivity, which leads to successful melting. Spreadability of the thin powder layer is conditioned by the powder particle properties, such as morphology, PSD, chemical composition and surface chemistry. The avalanche energy, break energy and cohesion (Figure 7a) and avalanche angle (Figure 7b) results per virgin and reused powder particles with a constant speed of 0.6 RPM, as suggested by Spierings et al. [22], are shown in Figure 7. The avalanche energy represents the amount of energy released by the collapse of an avalanche, while the break energy measures the resistance of the powder to flow. Cohesion-t is calculated from the shear stress created by the powder layer. This value gives an indication of whether the powder flows as individual particles or agglomerates. As shown in Figure 7, the flow behavior between the as-received (AR) and dried (D) powder is very similar at low speed with a slight tendency to worsen, but no large differences are observed, given the standard deviation. The drying treatment was intended to remove all humidity from the powder, as it is done by pre-heating the deposited layer during PBF-EB process. Alternately, the flow behavior and, therefore, spreadability show a clear improvement in all studied parameters from virgin to reused powder, as concluded by Snow et al. [23] when analyzing metrics to correlate both properties.

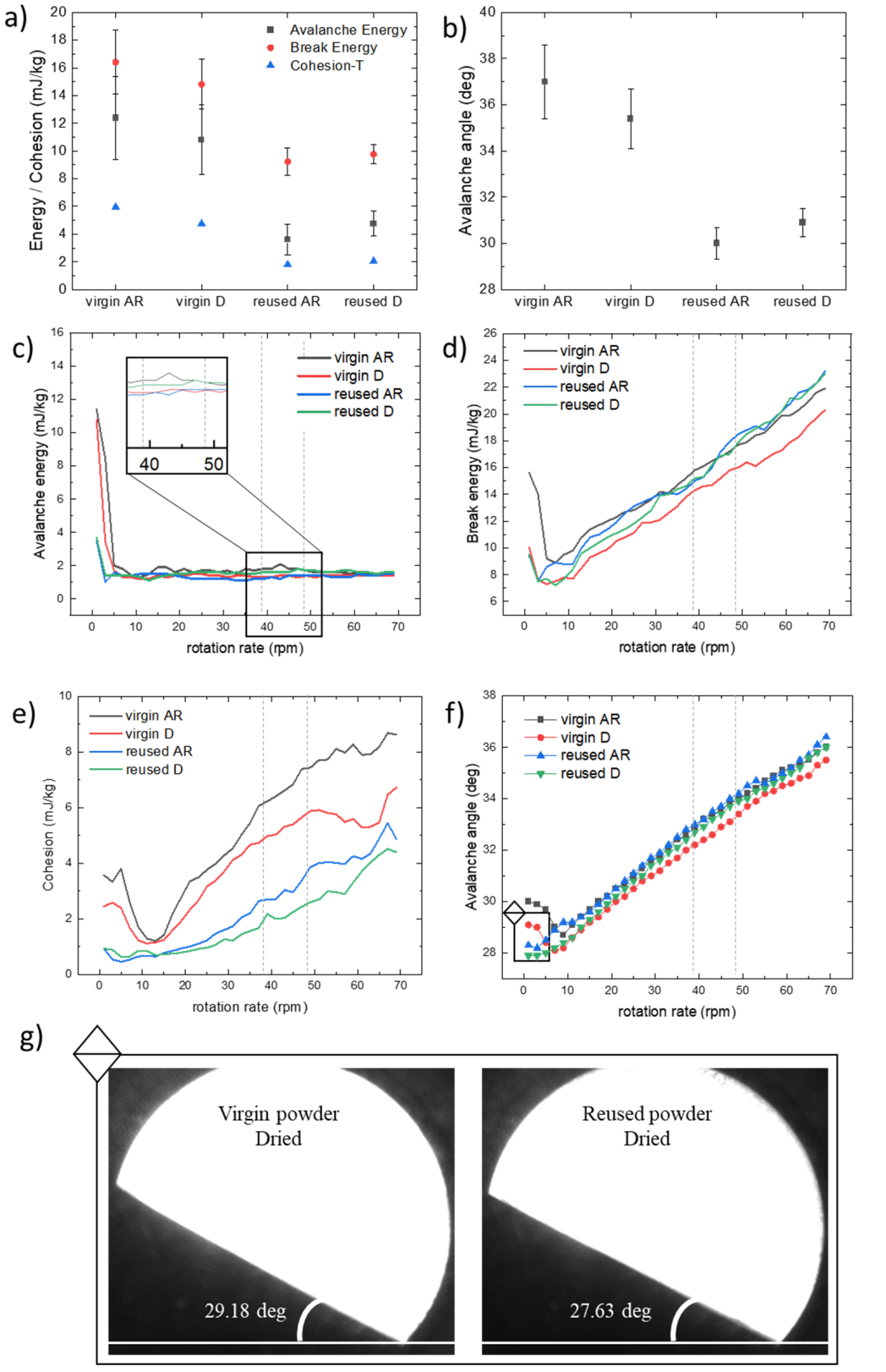

Figure 7. (**a**) Flowability metrics (avalanche energy, break energy and cohesion) and (**b**) avalanche angle using a constant speed of 0.6 RPM. Multi-flow test metrics (**c**) avalanche energy, (**d**) break energy, (**e**) cohesion and (**f**) avalanche angle. (**g**) Avalanche morphology at 1 RPM. All measurements show the behavior of virgin and reused powder in as-received (AR) and dried (D) condition.

Dynamic measurements with varying angular speed between 1 RPM and 69 RPM are shown in Figure 7c–f. The progressive change in the studied parameters from low to high angular speed can be appreciated. In this case, the range for angular speed relevant for the PBF-EB process is between 38 RPM and 48 RPM, which is equivalent to circa 200 mm/s to 250 mm/s, as converted by Equation (1). The avalanche angle, similar to the avalanche energy, break energy and cohesion parameters, shows an improved rheology in the reused powder sample, in comparison to the virgin one. The mechanisms that lead to the changes from low speed to high speed are associated with different forms of transverse motion of solids, which depend on the Froude number linked to the angular speed, as discussed by Mellmann et al. [24]. Changes observed in the range of angular velocities, around 10 RPM, are due to transitions between slumping and rolling or even cascading.

Independent of the angular speed, the powder avalanche maintains a straight line, which is commonly seen in powder with excellent flowability [25], as shown in Figure 7g. The image corresponds to low rotation speeds (1 RPM), the marked area on the graph in Figure 7f. At this point, the dried reused powder exhibits a slightly better flow behavior than the dried virgin powder.

3.5. Tap and Apparent Density

The apparent density of the powder was obtained during this experiment when the powder was in static mode, while the tap density of the powder was obtained by vibration and tapping of the powder volume. These values are used to calculate the loose and packed volume fraction, respectively, as shown in Table 3. The loose/packed volume fraction will determine the success of the powder particles packing on the build plate. From the values of Table 3, it can be concluded that the studied powders in virgin, reused, as-received and dried conditions show a large volume fraction, which would positively contribute to high powder packing.

Table 3. Apparent density, tap density measured by the RPA and relative density calculated using Equation (2).

Material	Apparent Density (g/cm^3)	Loose Volume Fraction (%)	Tap Density (g/cm^3)	Packed Volume Fraction (%)
Virgin AR	4.65 ± 0.03	56.69 ± 0.31	4.96 ± 0.05	60.50 ± 0.63
Virgin D	4.60 ± 0.02	56.08 ± 0.27	4.90 ± 0.07	59.73 ± 0.87
Reused AR	4.57 ± 0.02	55.71 ± 0.19	4.67 ± 0.02	57.02 ± 0.29
Reused D	4.55 ± 0.03	55.54 ± 0.42	4.82 ± 0.05	58.81 ± 0.63

3.6. Charging

The electrostatic charge results of the studied materials are presented in Figure 8. The overall charge (first 20 s of the experiment) reveals that the reused powder, both in as-received (AR) and dried (D) condition, acquires a higher maximum charge, which is almost double than for the virgin powder. The most important indication of a strongly charging powder is when the maximum charge is acquired fast, as happens with both reused powders. The next data points of the experiment will be determined by the amount of powder sticking to the glass, which might prevent a further increase or even a decay. Therefore, it is concluded that while drying does not necessarily affect the charging behavior, the powder reuse does. In this case, due to the oxide layer that is covered by Al rich in oxide particulates, as discussed in Section 3.3, the electrical conductivity between particles is affected, which is likely to be the cause of smoking in this reused powder.

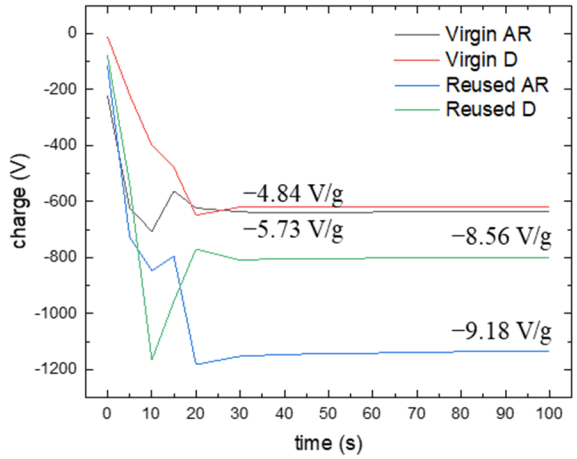

Figure 8. Electrostatic charge measurement of virgin and reused powder in as-received (AR) and dried (D) condition.

4. Discussion

4.1. Physical Properties of Reused Powder

As a summary of the presented results, the main differences between the virgin powder and the 'smoking' reused powder lays in the surface chemistry. This, at the same time, positively influences the flowability, although the tap density has not varied due to only minor changes in particle size and shape. The experimental methodology was designed to understand and characterize, at a deeper level, the cause of smoking in the reused powder. As expected, the charging behavior varies with changes in the oxide layer composition. The virgin surface was covered with a uniform oxide layer consisting of Ni, Cr and Fe-based oxides, which are less stable at higher temperatures. The reused powder surface was covered with stable Al-based oxide particulates. The formation of such particulates was triggered by higher stability of Al-based oxides at elevated temperature and redistribution of oxygen from already existing less stable oxide on the surface towards the stable oxides. This also explains the reason behind such a high coverage of Al-based oxide particulates on the surface of reused powder without a substantial increase in bulk oxygen content from virgin to reused powder. Given the change in chemistry and morphology of surface oxides, a variation in rheological and charging behavior from virgin to reused powders is expected.

The rheological metrics selected to characterize the flow behavior of the powders show improvements upon reuse. Avalanche angle, avalanche energy and break energy show reduced values, indicated as good flowing powders [26,27], which correlates as well with the cohesion results. The RPA offers a quantitative and qualitative rheological measurement that is sensitive to differences between virgin and reused powders. Tap density has shown a slight decrease in reused powder, despite the improvement in flow behavior, which can also lead to less optimal electrical conductivity between the powder particles, causing smoking. As shown in the schematic of Figure 9, the surface chemistry variation might impact the charging behavior of the powder to dissipate the electrons injected in the powder bed. As discussed by Galati and Iuliano [28], a pushing phenomenon of the powder particles can take place for different reasons: (i) humidity, (ii) momentum in the particles greater than cohesion and (iii) a negative electrostatic charge of the powder particles causing repulsive forces. The repulsive forces responsible for the particles negatively charge to repel themselves mutually [29]. This can be calculated using the Coulomb force, which is multiple-times larger than the normal force of a powder particle, leading to acceleration and ejection from the build envelope [30]. As Fu et al. [31] proposes in a smoking model, during the heating phase, if powder conductivity is high enough, there will be no change accumulation; this would be different when powders are covered by a thickened oxide layer by reuse. However, due to the presence of a vapor plume, some powder particles are lifted into the atmosphere due to evaporation pressure, initiating the so-called smoking effect.

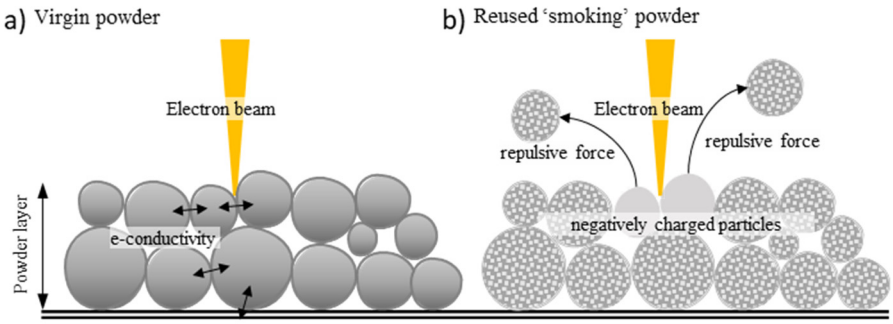

Figure 9. Schematic of powder deposition and interaction between particles of virgin (**a**) and reused (**b**) powder in PBF-EB.

4.2. Challenges in Processibility and Mitigation Actions

During six build cycles of powder reuse, Chandrasekar et al. [32] found additional powder spreading operations with increased reuse using rake position and rake sensor pulse data rake. In particular, Inconel 718 tends to agglomerate over multiple cycles of reuse. Additionally, Nandwana et al. [33] studied flowability using a hall flowmeter but did not detect changes in the free-flow behavior of the Inconel 718 powder during six cycles of reuse. However, this does not indicate that the changes in powder morphology have a large influence, as PBF-EB machine log data indicated variations in the spreading operations. In this study, the flow behavior of the powder upon reuse shows variations in comparison to the virgin powder. This variation could influence the spreading operations during the PBF-EB process. On the quality of the builds, the study by Gruber et al. [12] demonstrated a clear correlation between oxide inclusions with the increase in oxygen content due to powder reuse. Lack of fusion defects in samples built from reused powder could not be consolidated by hot isostatic pressing; this could affect the structural integrity of the parts [13].

It should be noted that, to prolong the powder life during reuse, different strategies can be applied. Some suggest adjusting the process parameters, such as beam focus and scanning speed, to process finer powder as proposed by Algardh et al. [34]. Another way to suppress smoking was studied by Cordero et al. [35] by modifying the resistivity of the powder overlayer, adjusting the alloy chemistry to produce more conductive oxide layers or grow ultrathin overlayers that electrons can surpass. Increasing the temperature of the build chambers is another way to suppress smoking. In addition, Chiba et al. [7] proposed a mechanical treatment by ball milling, given the dielectric–metallic transition the oxide layer is subjected to lattice strain. Smoking was suppressed even without pre-heating temperature. Different strategies, in situ and ex situ can be applied to condition the powder in between reuse cycles to prolong the life cycle while suppressing smoking.

5. Conclusions

In this study, virgin and reused powder processed by PBF-EB was studied, both in as-received and dried condition. The morphology, particle size distribution, bulk and surface chemistry of the powder was analyzed. The objective of the work is to successfully link powder smoking and degradation during reuse with the rheological and charging behavior. The following concluding remarks are listed:

- The morphology and particle size of the powder is mildly impacted by reuse and handling. A shift of circa 8% towards lower particle size values is observed. The morphology of reused powders exhibits less satellites and deformations from blasting.
- The bulk oxygen content of the powder increased by 20% upon reuse.
- The nature of the oxide layer and thickness varies from virgin to reused powder. Virgin powder was covered by a thin homogeneous oxide layer, formed preferably by Ni and Cr-oxide. In the case of reused powder, the powder surface was covered with Al-rich oxide particulates with average thicknesses around 13 nm according to XPS analysis.

- Reused powder exhibits better flowability motivated by changes in the oxide layer, measured by dynamic flowability metrics using the RPA. The loose volume fraction, equivalent to the packing density, is circa 57% and 56% for virgin and reused powders, respectively. When tapping, the packed volume fraction increased to 60% in virgin powders and to 57% in reused powder, the particulates and different surface roughness of the reused powder could be hindering a further packing, which could affect the thermal properties and, therefore, quality of the prints.
- The charging behavior of the powder varies in the reuse powders (-9.18 V/g) in comparison with the virgin powders (-5.84 V/g); it potentially offers less electrical conductivity, which is associated to smoking in the powder bed.
- No large differences were observed in rheological and charging behavior upon drying, confirmed by similar estimation of moisture by thermogravimetric analysis in both virgin and reused powders.

Author Contributions: Conceptualization, L.C. and A.R.; methodology, L.C.; formal analysis, L.C. and A.R.; investigation, L.C. and A.R.; writing—original draft preparation, L.C. and A.R.; writing—review and editing, E.H.; visualization, L.C.; supervision, E.H.; funding acquisition, E.H. All authors have read and agreed to the published version of the manuscript.

Funding: The work was performed in the framework of the Centre for Additive Manufacturing-Metal (CAM2) hosted by Chalmers University of Technology, supported by VINNOVA (grant number: 2016-05175).

Institutional Review Board Statement: Not applicable.

Informed Consent Statement: Not applicable.

Data Availability Statement: Not applicable.

Acknowledgments: The authors thank Höganäs AB for the particle size distribution and bulk composition analysis of the powder samples and Arcam AB for providing the powder materials.

Conflicts of Interest: The authors declare no conflict of interest.

References

1. Matz, J.E.; Eagar, T.W. Carbide formation in alloy 718 during electron-beam solid freeform fabrication. *Met. Mater. Trans. A* **2002**, *33*, 2559–2567. [CrossRef]
2. Helmer, H.E.; Körner, C.; Singer, R.F. Additive manufacturing of nickel-based superalloy Inconel 718 by selective electron beam melting: Processing window and microstructure. *J. Mater. Res.* **2014**, *29*, 1987–1996. [CrossRef]
3. Gibson, I.; Rosen, D.W.; Stucker, B. *Additive Manufacturing Technologies*; Springer US: New York, NY, USA, 2010.
4. Galati, M. Chapter 8-Electron beam melting process: A general overview. In *Additive Manufacturing*; Pou, J., Riveiro, A., Davim, J.P., Eds.; Elsevier: Amsterdam, The Netherlands, 2021; pp. 277–301.
5. Smith, C.J.; Tammas-Williams, S.; Hernández-Nava, E.; Todd, I. Tailoring the thermal conductivity of the powder bed in Electron Beam Melting (EBM) Additive Manufacturing. *Sci. Rep.* **2017**, *7*, 10514. [CrossRef] [PubMed]
6. Hryha, E.; Shvab, R.; Gruber, H.; Leicht, A.; Nyborg, L. Surface oxide state on metal powder and its changes during additive manufacturing: An overview. *Metall. Ital.* **2018**, *3*, 34–39.
7. Chiba, A.; Daino, Y.; Aoyagi, K.; Yamanaka, K. Smoke Suppression in Electron Beam Melting of Inconel 718 Alloy Powder Based on Insulator–Metal Transition of Surface Oxide Film by Mechanical Stimulation. *Materials* **2021**, *14*, 4662. [CrossRef]
8. Yi, F.; Zhou, Q.; Wang, C.; Yan, Z.; Liu, B. Effect of powder reuse on powder characteristics and properties of Inconel 718 parts produced by selective laser melting. *J. Mater. Res. Technol.* **2021**, *13*, 524–533. [CrossRef]
9. Cordova, L.; Campos, M.; Tinga, T. Revealing the Effects of Powder Reuse for Selective Laser Melting by Powder Characterization. *JOM* **2019**, *71*, 1062–1072. [CrossRef]
10. Gruber, H.; Henriksson, M.; Hryha, E.; Nyborg, L. Effect of Powder Recycling in Electron Beam Melting on the Surface Chemistry of Alloy 718 Powder. *Met. Mater. Trans. A* **2019**, *50*, 4410–4422. [CrossRef]
11. Raza, A.; Hryha, E. Characterization of Spatter and Sublimation in Alloy 718 during Electron Beam Melting. *Materials* **2021**, *14*, 5953. [CrossRef]
12. Gruber, H.; Luchian, C.; Hryha, E.; Nyborg, L. Effect of Powder Recycling on Defect Formation in Electron Beam Melted Alloy 718. *Met. Mater. Trans. A* **2020**, *51*, 2430–2443. [CrossRef]
13. Gruber, H.; Karimi, P.; Hryha, E.; Nyborg, L. Effect of Powder Recycling on the Fracture Behavior of Electron Beam Melted Alloy 718. *Powder Met. Prog.* **2018**, *18*, 40–48. [CrossRef]

14. Marchetti, L.; Hulme-Smith, C. Flowability of steel and tool steel powders: A comparison between testing methods. *Powder Technol.* **2021**, *384*, 402–413. [CrossRef]
15. Lefebvre, L.; Whiting, J.; Nijikovsky, B.; Brika, S.; Fayazfar, H.; Lyckfeldt, O. Assessing the robustness of powder rheology and permeability measurements. *Addit. Manuf.* **2020**, *35*, 101203. [CrossRef]
16. Vock, S.; Klöden, B.; Kirchner, A.; Weißgärber, T.; Kieback, B. Powders for powder bed fusion: A review. *Prog. Addit. Manuf.* **2019**, *4*, 383–397. [CrossRef]
17. Mussatto, A.; Groarke, R.; O'Neill, A.; Obeidi, M.A.; Delaure, Y.; Brabazon, D. Influences of powder morphology and spreading parameters on the powder bed topography uniformity in powder bed fusion metal additive manufacturing. *Addit. Manuf.* **2020**, *38*, 101807. [CrossRef]
18. Strondl, A.; Lyckfeldt, O.; Brodin, H.; Ackelid, U. Characterization and Control of Powder Properties for Additive Manufacturing. *JOM* **2015**, *67*, 549–554. [CrossRef]
19. Cordova, L.; Bor, T.; de Smit, M.; Campos, M.; Tinga, T. Measuring the spreadability of pre-treated and moisturized powders for laser powder bed fusion. *Addit. Manuf.* **2020**, *32*, 101082. [CrossRef]
20. Hulme-Smith, C.N.; Hari, V.; Mellin, P. Spreadability Testing of Powder for Additive Manufacturing. *BHM Berg Hüttenmännische Mon.* **2021**, *166*, 9–13. [CrossRef]
21. Baer, D.R.; Engelhard, M.H.; Lea, A.S.; Nachimuthu, P.; Droubay, T.C.; Kim, J.; Lee, B.; Mathews, C.; Opila, R.L.; Saraf, L.V.; et al. Comparison of the sputter rates of oxide films relative to the sputter rate of SiO_2. *J. Vac. Sci. Technol. A Vac. Surf. Film.* **2010**, *28*, 1060–1072. [CrossRef]
22. Spierings, A.B.; Voegtlin, M.; Bauer, T.; Wegener, K. Powder flowability characterisation methodology for powder-bed-based metal additive manufacturing. *Prog. Addit. Manuf.* **2015**, *1*, 9–20. [CrossRef]
23. Snow, Z.; Martukanitz, R.; Joshi, S. On the development of powder spreadability metrics and feedstock requirements for powder bed fusion additive manufacturing. *Addit. Manuf.* **2019**, *28*, 78–86. [CrossRef]
24. Mellmann, J. The transverse motion of solids in rotating cylinders—Forms of motion and transition behavior. *Powder Technol.* **2001**, *118*, 251–270. [CrossRef]
25. Montes, B.C.; Martínez-Alejo, J.; Lozano-Perez, H.; Gumy, J.; Zemlyanov, D.; Carvajal, M. A surface characterization platform approach to study Flowability of food powders. *Powder Technol.* **2019**, *357*, 269–280. [CrossRef]
26. Goh, H.P.; Heng, P.W.S.; Liew, C.V. Comparative evaluation of powder flow parameters with reference to particle size and shape. *Int. J. Pharm.* **2018**, *547*, 133–141. [CrossRef]
27. Trpělková, Ž.; Hurychová, H.; Kuentz, M.; Vraníková, B.; Šklubalová, Z. Introduction of the energy to break an avalanche as a promising parameter for powder flowability prediction. *Powder Technol.* **2020**, *375*, 33–41. [CrossRef]
28. Galati, M.; Iuliano, L. A literature review of powder-based electron beam melting focusing on numerical simulations. *Addit. Manuf.* **2018**, *19*, 1–20. [CrossRef]
29. Milberg, J.; Sigl, M. Electron beam sintering of metal powder. *Prod. Eng.* **2008**, *2*, 117–122. [CrossRef]
30. Kahnert, M.; Lutzmann, S.; Zaeh, M.F. Layer Formations in Electron Beam Sintering. In Proceedings of the 18th Solid Freeform Fabrication Symposium, Austin, TX, USA, 6–8 August 2007; pp. 88–99.
31. Fu, Z.; Körner, C. Actual state-of-the-art of electron beam powder bed fusion. *Eur. J. Mater.* **2022**, *2*, 54–117. [CrossRef]
32. Chandrasekar, S.; Coble, J.B.; Yoder, S.; Nandwana, P.; Dehoff, R.R.; Paquit, V.C.; Babu, S.S. Investigating the effect of metal powder recycling in Electron beam Powder Bed Fusion using process log data. *Addit. Manuf.* **2019**, *32*, 100994. [CrossRef]
33. Nandwana, P.; Peter, W.H.; Dehoff, R.; Lowe, L.E.; Kirka, M.M.; Medina, F.; Babu, S. Recyclability Study on Inconel 718 and Ti-6Al-4V Powders for Use in Electron Beam Melting. *Met. Mater. Trans. A* **2015**, *47*, 754–762. [CrossRef]
34. Algardh, J.K.; Horn, T.; West, H.; Aman, R.; Snis, A.; Engqvist, H.; Lausmaa, J.; Harrysson, O. Thickness dependency of mechanical properties for thin-walled titanium parts manufactured by Electron Beam Melting (EBM)®. *Addit. Manuf.* **2016**, *12*, 45–50. [CrossRef]
35. Cordero, Z.C.; Meyer, H.M.; Nandwana, P.; Dehoff, R.R. Powder bed charging during electron-beam additive manufacturing. *Acta Mater.* **2017**, *124*, 437–445. [CrossRef]